Various Attractors, Coexisting Attractors and Antimonotonicity in a Simple Fourth-Order Memristive Twin-T Oscillator

Article *in* International Journal of Bifurcation and Chaos · April 2018

DOI: 10.1142/S0218127418500505

CITATIONS
2

READS
49

4 authors, including:

Ling Zhou
Hunan University
9 PUBLICATIONS **62** CITATIONS

SEE PROFILE

Chunhua Wang
Hunan University
167 PUBLICATIONS **792** CITATIONS

SEE PROFILE

International Journal of Bifurcation and Chaos, Vol. 28, No. 4 (2018) 1850050 (18 pages)

DOI: 10.1142/S0218127418500505

Various Attractors, Coexisting Attractors and Antimonotonicity in a Simple Fourth-Order Memristive Twin-T Oscillator

Ling Zhou*, Chunhua Wang†, Xin Zhang‡ and Wei Yao§
College of Computer Science and Electronic Engineering, Hunan University, Changsha 410082, P. R. China
**Department of Electronic and Information Engineering, Hunan University of Science and Engineering, Yongzhou 425199, P. R. China*
**zhouling0340@163.com*
†*wch1227164@hnu.edu.cn*
‡*zhangxin2302@126.com*
§*yaowei520026@sina.com*

Received October 19, 2017; Revised January 4, 2018

By replacing the resistor in a Twin-T network with a generalized flux-controlled memristor, this paper proposes a simple fourth-order memristive Twin-T oscillator. Rich dynamical behaviors can be observed in the dynamical system. The most striking feature is that this system has various periodic orbits and various chaotic attractors generated by adjusting parameter b. At the same time, coexisting attractors and antimonotonicity are also detected (especially, two full Feigenbaum remerging trees in series are observed in such autonomous chaotic systems). Their dynamical features are analyzed by phase portraits, Lyapunov exponents, bifurcation diagrams and basin of attraction. Moreover, hardware experiments on a breadboard are carried out. Experimental measurements are in accordance with the simulation results. Finally, a multi-channel random bit generator is designed for encryption applications. Numerical results illustrate the usefulness of the random bit generator.

Keywords: Twin-T oscillator; memristor; antimonotonicity; various attractors; random bit generator; encryption.

1. Introduction

Memristor, as the fourth basic circuit element, postulated in 1971 is a nonlinear two-terminal electronic element [Chua, 1971]. Generalized memristive systems have been proposed by Prof. Chua in 1976, and the most salient feature of memristive systems is its zero-crossing property [Chua & Kang, 1976]. Since the physical memristor has been fabricated by Hewlett-Packard Lab in 2008 [Strukov *et al.*, 2008], it has attracted much attention of researchers. Due to its nonvolatility, nanosize, and low power consumption, memristor can be applied in various fields, such as nonvolatile memory [Strukov, 2016], neural networks [Soudry *et al.*, 2015; Duan *et al.*, 2015], nonlinear chaotic circuits [Zhou *et al.*, 2016; Wu & Wang, 2016; Yuan *et al.*, 2016; Wang *et al.*, 2017; Corinto & Forti, 2017; Ma *et al.*, 2017], and so on.

†Author for correspondence

Oscillators are frequently used as signal generators. It is thought that chaotic signal generation with wide frequency spectrum has potential application for secure communication and image encryption [Ren *et al.*, 2017; Lin *et al.*, 2016; Li *et al.*, 2017]. In addition, the long-term unpredictability of chaotic signal makes these systems well suited for true random bit generation [Yalcin *et al.*, 2004]. In robotics, chaotic signals are being used in neural control networks or as chaotic path generators [Li *et al.*, 2015]. In all these applications, they need to exist for flexible, preferably low-cost chaotic circuits. A large number of chaotic oscillators were reported [Morgul, 1995; Namajunas & Tamasevicius, 1996; Iu *et al.*, 2010; Elwakil & Kennedy, 2000; Keuninckx *et al.*, 2015]. By substituting nonlinear element or linear element with memristor in classic oscillators, memristive oscillators with complex dynamical behaviors have been recently discussed [Iu *et al.*, 2011; Bao *et al.*, 2015; Xu *et al.*, 2016; Chen *et al.*, 2015; Yu *et al.*, 2014b; Wu *et al.*, 2016; Bao *et al.*, 2016, 2017a].

By replacing the Chua diode with memristor in Chua's circuit consisting of inductor, the rich varieties of bifurcation structures are analyzed [Bao *et al.*, 2015; Xu *et al.*, 2016; Chen *et al.*, 2015]. The Wien-bridge nonlinear oscillator composed of a Wien-bridge oscillator, memristor, and LC network is proposed, and there exist complex nonlinear phenomena including periodic oscillations, chaotic oscillations and fast–slow effects [Yu *et al.*, 2014b]. In 2016, a simple memristive Wien-bridge oscillator is constituted by replacing the resistor of parallel RC network with generalized memristor [Wu *et al.*, 2016]; however, the generalized memristor contains LC network. The above memristive oscillators all include inductor [Iu *et al.*, 2011; Bao *et al.*, 2015; Xu *et al.*, 2016; Chen *et al.*, 2015; Yu *et al.*, 2014b; Wu *et al.*, 2016]. It is well known that the presence of an inductor with parasitic equivalent series resistor makes circuit hardware bulky, unsuitable for IC design, less robust, etc. Later, by linearly coupling a parallel memristor and capacitor filter to a single amplifier biquad-based inductor-free Chua's circuit with an ideal memristor [Bao *et al.*, 2016], or by replacing a nonlinear resistor and a linear resistor with two different memristors in an active band pass filter-based Chua's circuit [Bao *et al.*, 2017a], extreme multistability and other complex dynamical behaviors are discussed.

In 2014, by substituting the resistor with memristor, the memristive relaxation oscillator provides novel and steady oscillating behaviors [Yu *et al.*, 2014a], however, it cannot generate a chaotic signal. In 2010, chaos in a Twin-T circuit is described, and the circuit is very simple, requiring just one opamp stage. However, the circuit must be driven by a low frequency input-signal [Iu *et al.*, 2010]. A five-order inductor-free nonlinear oscillator composed of a Twin-T oscillator, memristor, and RC network is designed [Li & Zeng, 2013].

In this paper, a generalized memristor is used to directly replace the resistor in a Twin-T oscillator. Compared with the reference [Iu *et al.*, 2010], the proposed chaotic circuit does not need extra input-signal. At the same time, compared with the work [Li & Zeng, 2013], the proposed Twin-T oscillator with memristor, keeping the original oscillator circuit structure, does not need to add extra RC network. Moreover, it has a relatively simpler electronic structure (absence of RC network) and complex dynamical behaviors. Compared to former work reported [Iu *et al.*, 2010; Elwakil & Kennedy, 2000; Li & Zeng, 2013], the new memristive Twin-T system has various periodic orbits and various chaotic attractors by adjusting parameter b. Only adjusting the Resistor R_2, therefore, it is convenient and easy in different oscillator applications. Moreover, it has also many interesting properties such as series antimonotonicity, and coexisting attractors. Although the phenomenon of antimonotonicity is observed in many circuits, as far as I know, antimonotonicity (two full Feigenbaum remerging trees in series) is less observed in the autonomous chaotic systems.

The paper is organized as follows. In Sec. 2, the circuit structure of the memristive Twin-T oscillator is depicted, and a suitable mathematical model is obtained. In Sec. 3, some basic properties of the mathematical model such as dissipativity, equilibrium, and stability are analyzed. In Sec. 4, simulation analyses of the dynamical system are investigated by phase portraits, bifurcation diagram and Lyapunov exponents. Many various periodic attractors, various chaotic attractors, coexisting attractors (for the same parameter settings) and antimonotonicity are discussed. In Sec. 5, hardware experiments on a breadboard are carried out. In Sec. 6, a random bit generator design with the memristive Twin-T chaotic system is proposed, the three

outputs of the memristive Twin-T oscillator all successfully pass all the tests NITS-800-22. The conclusive remarks are finally drawn in Sec. 7.

2. Circuit Description

By substituting the resistor in Twin-T oscillator with memristor, the new proposed memristive Twin-T oscillator is depicted in Fig. 1.

Due to the memristor being not commercially available, various kinds of memristive emulators have been proposed for studying the application circuits of memristor. According to the form of generalized voltage-controlled memristor defined by Chua in [Chua & Kang, 1976], the emulator proposed by Bao and co-workers [Bao *et al.*, 2017b] only has eight elements and can be easily physically implemented, as shown in Fig. 2, where v and i stand for the voltage and the current at the input port of memristor, respectively, V_φ denotes the voltage across the integral capacitor C_φ, and g denotes the scale factor of multiplier. The voltage–current relationship of the memristor emulator is modeled as

$$\begin{aligned} i = W(V_\varphi)v &= \frac{v - gv(gV_\varphi^2)}{R_\varphi} \\ &= \frac{1}{R_\varphi}(1 - g^2V_\varphi^2)v \end{aligned} \tag{1}$$

$$\frac{\mathrm{d}V_\varphi}{\mathrm{d}t} = f(V_\varphi, v) = -\frac{V_\varphi}{R_{m2}C_\varphi} - \frac{v}{R_{m1}C_\varphi}$$

where $W(V_\varphi)$ is a continuous linear memductance function related to V_φ, which can be given by

$$W(V_\varphi) = \frac{1}{R_\varphi}(1 - g^2V_\varphi^2). \tag{2}$$

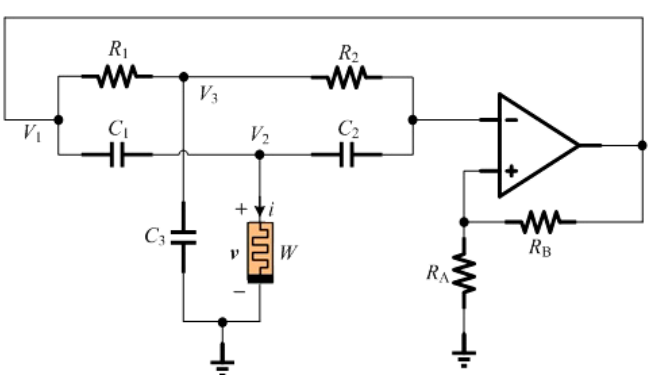

Fig. 1. The proposed Twin-T oscillator with memristor.

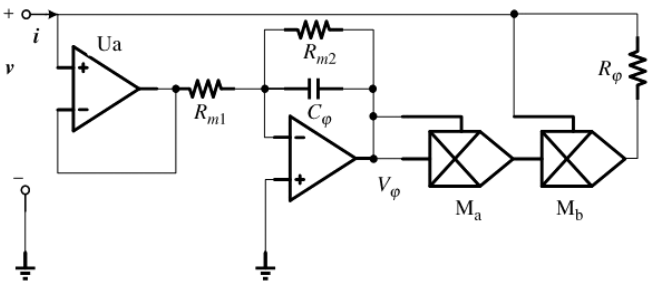

Fig. 2. The memristor emulator.

The circuit parameters in Figs. 1 and 2 are given in Table 1. Due to the absence of RC network, the new proposed memristive Twin-T chaotic circuit is a fourth-order nonlinear circuit. According to the constitutive relation of memristor and the KVL equations of Twin-T chaotic circuit, the dynamical equations of memristive Twin-T chaotic circuit in Fig. 1 can be described as

$$\begin{aligned} C_1\frac{\mathrm{d}V_1}{\mathrm{d}t} &= (1+k)\frac{1}{R_\varphi}(1 - g^2V_\varphi^2)V_2 \\ &\quad - \frac{2V_3(1+k)}{R_2} + \frac{2kV_1}{R_2} \\ C_2\frac{\mathrm{d}V_2}{\mathrm{d}t} &= k\frac{1}{R_\varphi}(1 - g^2V_\varphi^2)V_2 \\ &\quad - \frac{V_3(1+2k)}{R_2} + \frac{(2k+1)kV_1}{R_2(1+k)} \\ C_3\frac{\mathrm{d}V_3}{\mathrm{d}t} &= \frac{V_1}{R_1} + \frac{kV_1}{R_2(1+k)} - \frac{V_3}{R_1} - \frac{V_3}{R_2} \\ C_\varphi\frac{\mathrm{d}V_\varphi}{\mathrm{d}t} &= -\frac{V_2}{R_{m1}} - \frac{V_\varphi}{R_{m2}} \end{aligned} \tag{3}$$

Table 1. Element parameters of memristive Twin-T oscillator.

Parameters	Significations	Values
C_1, C_2, C_3, C_φ	Capacitance	10 nF
R_φ	Resistance	13.3 kΩ
R_1	Resistance	28.57 kΩ
R_2	Resistance	285.7 kΩ
R_{m1}	Resistance	10 kΩ
R_{m2}	Resistance	100 kΩ
R_A	Resistance	1 kΩ
R_B	Resistance	10 kΩ

where $k = R_A/R_B$, V_1, V_2, V_3 and V_φ are four node voltages standing for four state variables.

Let $t = \tau \mathrm{RC}$, where τ is the dimensionless time. The parameters are expressed as follows:

$$\begin{aligned} x = V_1, \quad y = V_2, \quad z = V_3, \quad u = V_\varphi, \\ C_1 = C_2 = C_3 = C, \\ a = \frac{R}{R_\varphi}, \quad b = \frac{R}{R_2}, \quad c = \frac{R}{R_1}, \\ m = \frac{RC}{R_{m1}C_\varphi}, \quad n = \frac{RC}{R_{m2}C_\varphi}. \end{aligned} \tag{4}$$

Therefore, the dimensionless equations can be described as follows:

$$\begin{aligned} \dot{x} &= (1+k)a(1-g^2u^2)y \\ &\quad - 2(1+k)bz + 2kbx \\ \dot{y} &= ka(1-g^2u^2)y - (1+2k)bz \\ &\quad + \frac{(2k+1)bkx}{1+k} \\ \dot{z} &= cx + \frac{bkx}{1+k} - cz - bz \\ \dot{u} &= -my - nu. \end{aligned} \tag{5}$$

When $R = 100\,\mathrm{k\Omega}$ and $C = 10\,\mathrm{nF}$, the numerical experiment is carried out with the following dimensionless parameters: $a = 7.5$, $b = 0.35$, $c = 3.5$, $m = 10$, $n = 1$, $k = 0.1$, $g = 0.1$.

3. Dissipativity, Equilibrium, and Stability

It can be observed obviously that the system (5) is symmetrical about the origin and invariant under the transformation $(x, y, z, u) \to (-x, -y, -z, -u)$, which indicates that if (x, y, z, u) is a solution of (5), then $(-x, -y, -z, -u)$ is also a solution.

To evaluate the dissipativity of system (5), the mathematical expression of exponential constrain rate is deduced as

$$\begin{aligned} \nabla V &= \frac{\partial \dot{x}}{\partial x} + \frac{\partial \dot{y}}{\partial y} + \frac{\partial \dot{z}}{\partial z} + \frac{\partial \dot{\varphi}}{\partial \varphi} \\ &= ka(1-g^2u^2) + 2kb - c - b - n. \end{aligned} \tag{6}$$

When $ka < c + b + n - 2kb$, (6) is negative, i.e. $\triangle V < 0$, implying that the system is dissipative. This means that asymptotic motion settles onto an attractor and each volume containing the system trajectory shrinks to zero at an exponential rate as $t \to \infty$.

The equilibria of system (5) can be derived by solving the following equations:

$$\begin{cases} (1+k)a(1-g^2u^2)y - 2(1+k)bz + 2kbx = 0 \\ ka(1-g^2u^2)y - (1+2k)bz + \dfrac{(2k+1)bkx}{1+k} = 0 \\ cx + \dfrac{bkx}{1+k} - cz - bz = 0 \\ -my - nu = 0. \end{cases} \tag{7}$$

We can easily observe that the system (5) has three equilibrium points including one zero equilibrium and two symmetric nonzero equilibria, which are described by:

$$\begin{aligned} P_0 &= (0, 0, 0, 0), \\ P_\pm &= \left(0, \mp\frac{n}{mg}, 0, \pm\frac{1}{g}\right). \end{aligned} \tag{8}$$

By linearizing system (5) at zero equilibrium P_0, we can obtain the Jacobian matrix.

$$Jo = \begin{pmatrix} 2kb & (1+k)a & -2(1+k)b & 0 \\ \dfrac{(2k+1)kb}{1+k} & ka & -(1+2k)b & 0 \\ c + \dfrac{bk}{1+k} & 0 & -(c+b) & 0 \\ 0 & -m & 0 & -n \end{pmatrix} \tag{9}$$

$$\begin{aligned} &\det(\lambda I - J_0) \\ &\quad = (\lambda + n)(\lambda^3 + a_1\lambda^2 + a_2\lambda + a_3) = 0 \\ &a_1 = c + b - ak - 2bk \\ &a_2 = 2bc - ack - 2abk \\ &a_3 = -(4abck^2 + 4ab^2k^2 + 6abck \\ &\quad + 2ab^2k + abc). \end{aligned} \tag{10}$$

The coefficients of the cubic polynomial equation of (10) are all nonzero, and the Routh–Hurwitz conditions for the above cubic polynomial are given

by

$$\begin{aligned} &a_1 > 0 \\ &a_3 > 0 \\ &a_1 a_2 - a_3 > 0. \end{aligned} \tag{11}$$

It is found that when the parameters of system (5) are all positive, a_3 is always negative, and the Routh–Hurwitz conditions are not satisfied. When the parameters of system (5) are taken as $a = 7.5$, $b = 0.35$, $c = 3.5$, $m = 10$, $n = 1$, $k = 0.1$, and $g = 0.1$, the eigenvalues at P_0 are calculated as

$$\begin{aligned} P_0 :\ &\lambda_1 = -1, \\ &\lambda_{2,3} = 0.4033 \pm 1.4940i, \\ &\lambda_4 = -3.8366 \end{aligned} \tag{12}$$

which implies that P_0 is an unstable saddle-focus.

Similarly, the Jacobian matrix at two nonzero equilibria $P_\pm$ can be deduced as

$$J_\pm = \begin{pmatrix} 2kb & 0 & -2(1+k)b & \dfrac{2an(1+k)}{m} \\ \dfrac{(2k+1)kb}{1+k} & 0 & -(1+2k)b & \dfrac{2akn}{m} \\ c + \dfrac{bk}{1+k} & 0 & -(c+b) & 0 \\ 0 & -m & 0 & -n \end{pmatrix} \tag{13}$$

$$\begin{aligned} &\det(\lambda I - J_\pm) \\ &\quad = \lambda^4 + a_1\lambda^3 + a_2\lambda^2 + a_3\lambda + a_4 = 0 \\ &a_1 = c + n + b - 2bk \\ &a_2 = 2bc + 2akn + cn + bn - 2bnk \\ &a_3 = 2ackn - 8abk^2n + 2bcn \\ &a_4 = -(8abcnk^2 + 8anb^2k^2 + 4abcnk \\ &\quad + 4anb^2k + 2abcn). \end{aligned} \tag{14}$$

The coefficients of the quartic polynomial equation of (14) are all nonzero, and the Routh–Hurwitz conditions for the above quartic polynomial are given by

$$\begin{aligned} &a_1 > 0 \\ &a_4 > 0 \\ &a_1 a_2 - a_3 > 0 \\ &a_1(a_3 a_2 - a_4 a_1) - a_1^2 > 0. \end{aligned} \tag{15}$$

It is found that when the parameters of system (5) are all positive, a_4 is always negative, and the Routh–Hurwitz conditions are not satisfied. When the parameters of system (5) are taken as $a = 7.5$, $b = 0.35$, $c = 3.5$, $m = 10$, $n = 1$, $k = 0.1$, and $g = 0.1$, the eigenvalues at $P_\pm$ are calculated as

$$\begin{aligned} P_\pm :\ &\lambda_1 = -3.6932, \\ &\lambda_{2,3} = -0.9947 \pm 2.1266i, \\ &\lambda_4 = 0.9026 \end{aligned} \tag{16}$$

which implies that $P_\pm$ has an unstable saddle.

4. Numerical Simulation of Twin-T Oscillator

4.1. *Various periodic orbits and various chaotic attractors*

The parameter b (Resistor R_2) will be considered as the main bifurcation control parameter in this work, and the others of system (5) are taken as $a = 7.5, c = 3.5, m = 10, n = 1, k = 0.1$, and $g = 0.1$. Changing the parameter b from 0.08 to 0.6 and setting the initial conditions ([1 0 0 0] and [−1 0 0 0]), we can obtain bifurcation diagrams in Fig. 3(a). First three Lyapunov exponents are shown in Fig. 3(b) when the initial condition is (1 0 0 0).

From the bifurcation diagrams, we can observe clearly that the system (5) has complex dynamic behaviors. When the parameters of system (5) are taken as $a = 7.5, c = 3.5, m = 10, n = 1, k = 0.1$, and $g = 0.1$, various attractors can be observed by changing the value of parameter b. Two parameter spaces will be considered in the following.

(1) $0.08 < b < 0.18$

Changing b from 0.08 to 0.18, the bifurcation diagrams of u (the interval of b is [0.08, 0.18]) are depicted in Fig. 4(a) and partial enlargement of bifurcation diagrams are depicted in Fig. 4(b). Along with increase of b in the interval [0.08, 0.18],

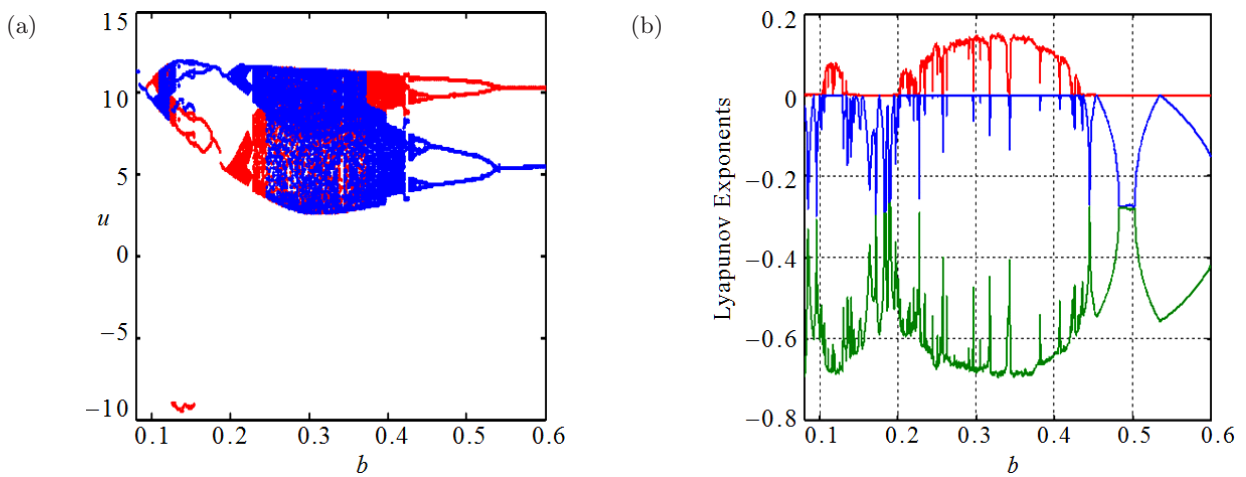

Fig. 3. Bifurcation diagrams and first three Lyapunov exponents: (a) Bifurcation diagrams of u, the red trajectories start from the initial conditions $(-1, 0, 0, 0)$, and the blue trajectories emerge from $(1, 0, 0, 0)$ and (b) first three Lyapunov exponents with respect to b when the initial condition is (1 0 0 0).

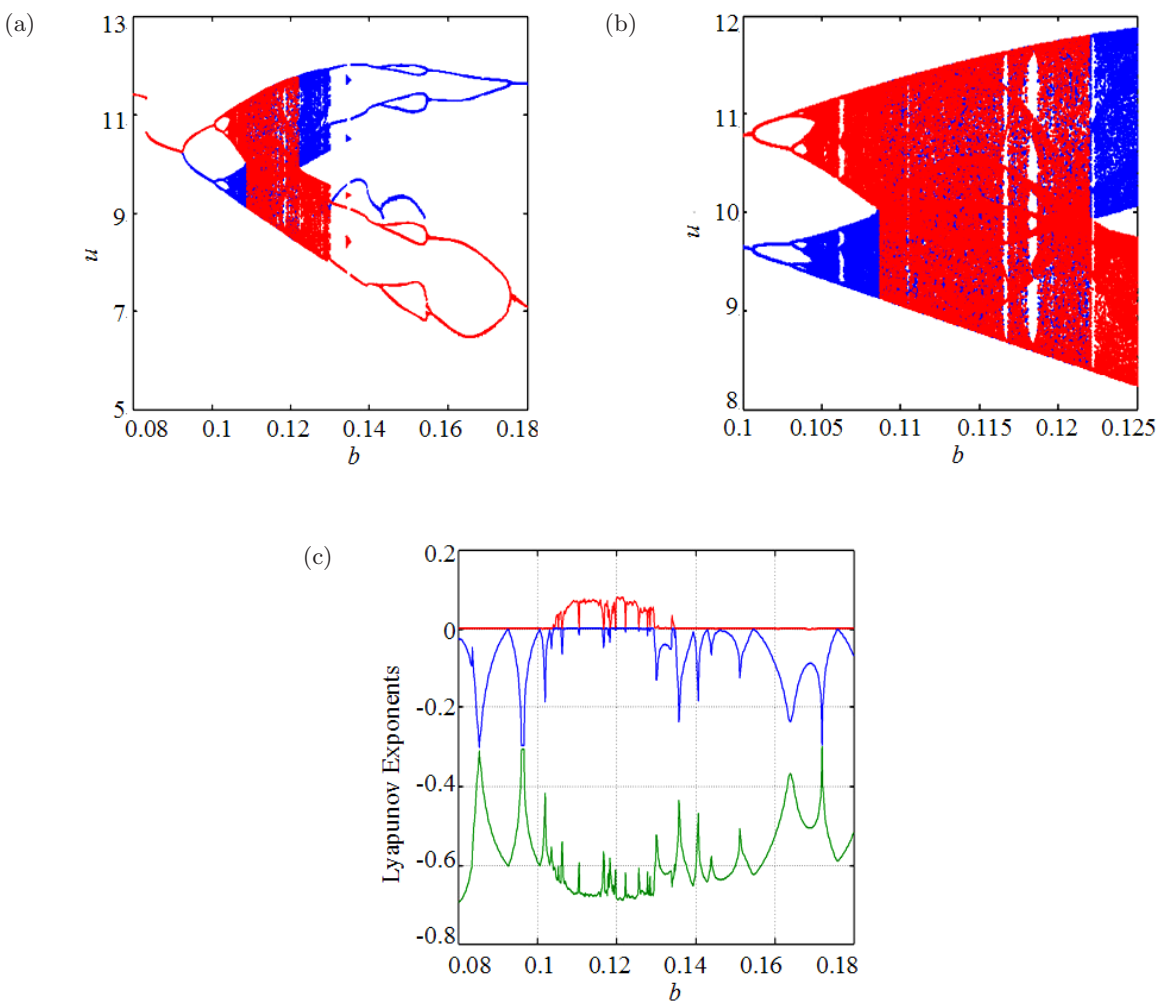

Fig. 4. Bifurcation diagrams and first three Lyapunov exponents (the interval of b is [0.08, 0.18]): (a) Bifurcation diagrams of u, the red trajectories start from the initial conditions $(-1, 0, 0, 0)$, and the blue trajectories emerge from $(1, 0, 0, 0)$, (b) the partial enlargement of (a) and (c) first three Lyapunov exponents with respect to b when the initial condition is (1 0 0 0).

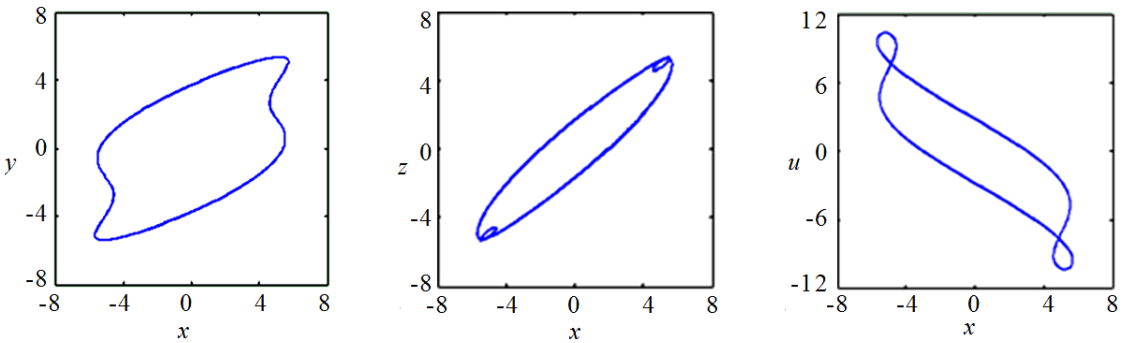

(a) (b) (c)

Fig. 5. Typical period-1 orbits in fourth-order memristive oscillator with Twin-T when $b = 0.09$: Phase portrait in the (a) x–y plane, (b) x–z plane and (c) x–u plane.

the orbits transform from coexisting period-1 to period-2 to period-4 and to period-8 successively. Furthermore, three main periodic windows with period-3, period-7 and period-9 appear in the intervals [0.1061, 0.1062], [0.1182, 0.1183] and [0.1166, 0.1167]. The corresponding first three Lyapunov exponents with respect to b are depicted in Fig. 4(c) when the initial conditions are (1, 0, 0, 0). The typical periodic orbits are shown in Fig. 5 when $b = 0.09$, and the typical chaotic attractors are shown in Fig. 6 when $b = 0.11$. When in the intervals [0.093, 0.109] and [0.129, 0.13], coexisting bifurcation modes appear, and the coexisting attractors are shown in Fig. 7.

(2) $0.18 < b < 0.6$

From the bifurcation diagrams in Fig. 3, there exist coexisting period orbits, chaotic attractors, and coexisting chaotic attractors. The typical chaotic attractors which are different from Fig. 6 are shown in Fig. 8 when $b = 0.3$. When in the intervals [0.18, 0.24] and [0.38, 0.6], coexisting bifurcation modes appear, and the coexisting attractors are shown in Fig. 9.

From the Figs. 5–9, this new system has various periodic orbits and various chaotic attractors by adjusting parameter b. Rich dynamical behaviors can be triggered in the dynamical system (5).

4.2. *Basins of attraction*

More information about the coexisting attractors can be obtained by analyzing the basins of attraction of the different attracting sets, which are defined as the set of initial conditions whose trajectories converge to the respective attractor [Li & Sprott, 2013]. In order to understand coexisting attractor, the basin of attraction is discussed. Take the coexisting chaotic attractors in Figs. 7(f) and 9(f) as examples, their basin boundaries are clearly observed in Fig. 10 where cross-sections of the basins of attraction for $y(0) = u(0) = 0$. Blue

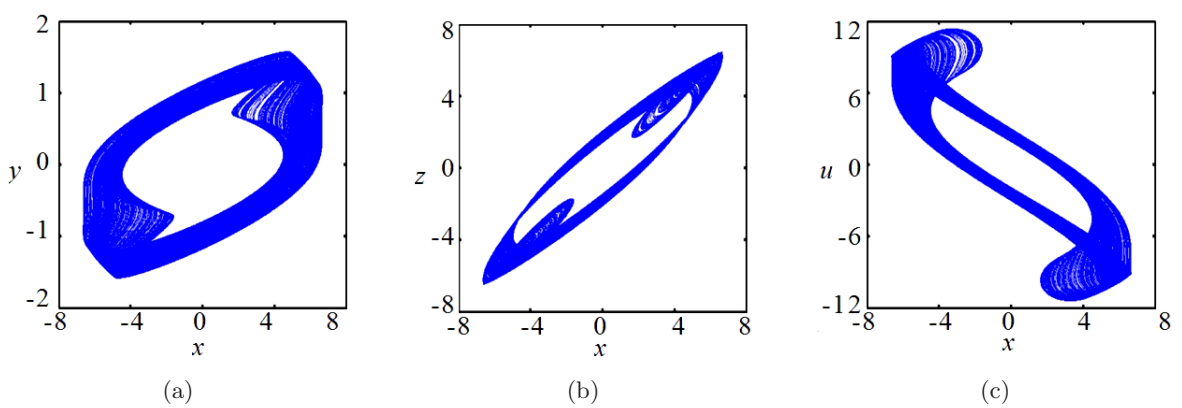

(a) (b) (c)

Fig. 6. Typical chaotic attractors in fourth-order memristive oscillator with Twin-T when $b = 0.11$: Phase portrait in the (a) x–y plane, (b) x–z plane and (c) x–u plane.

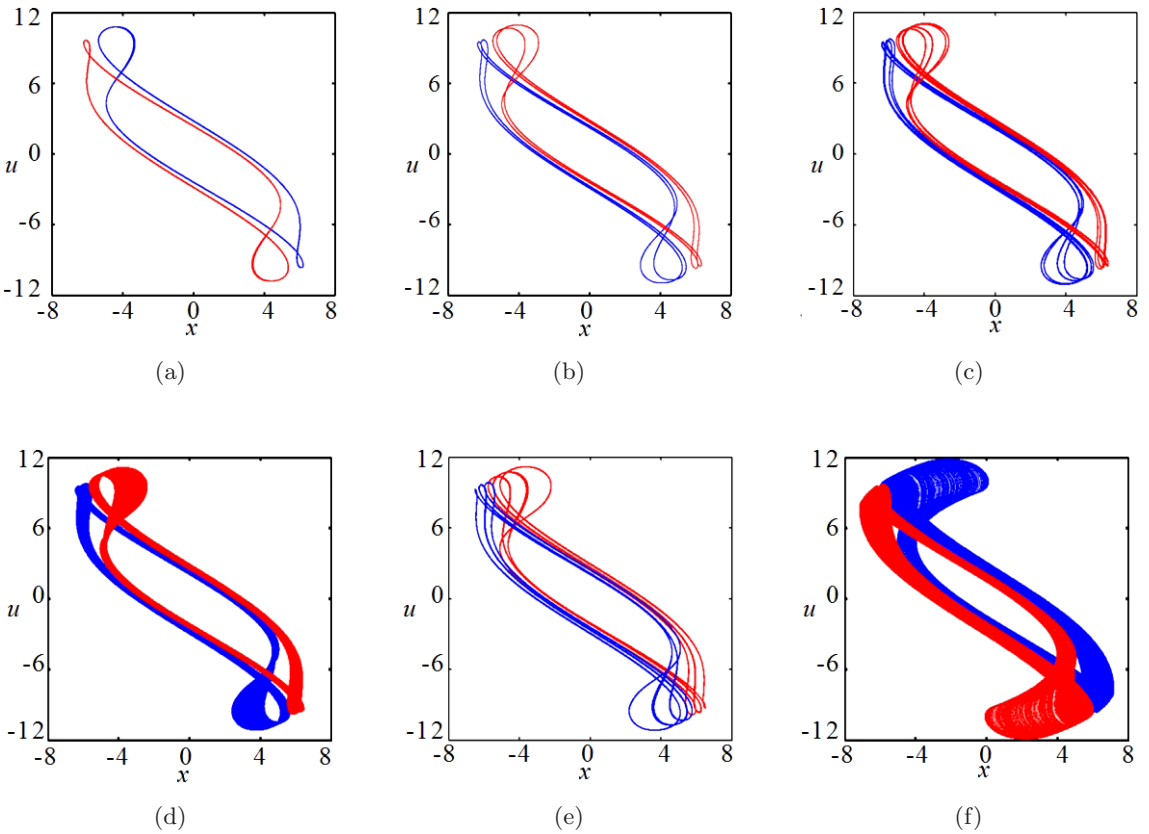

Fig. 7. The coexisting attractors in the x–u plane: (a) period-1 ($b = 0.1$), (b) period-2 ($b = 0.101$), (c) period-4 ($b = 0.1037$), (d) chaotic attractor ($b = 0.105$), (e) period-3 ($b = 0.1062$) and (f) chaotic attractor ($b = 0.125$).

and red zones denote the asymmetric pair of chaotic attractors. Green zones denote unbounded motion. From Fig. 10(a), it can be seen that there are two coexisting attractors shown in Fig. 7(f) when $b = 0.125$; however, there exists the third coexisting attractor except that it is shown in Fig. 9(f) when $b = 0.24$. In Fig. 10(b), yellow zones denote the third coexisting attractor when $b = 0.24$. The initial conditions of the third coexisting attractor are obtained in the progress of computing a basin of attraction (the corresponding yellow points' coordinates denote the initial conditions x_0 and z_0, respectively), therefore, the third coexisting attractor has strict initial condition. When the initial conditions are $(-0.025125628140704,\ 0,\ -4.547738693467337,\ 0)$, the phase portrait in the x–u plane is shown in Fig. 11(a). Based on the first three Lyapunov exponents depicted in Fig. 11(b), the third coexisting attractor when $b = 0.24$, is also a chaotic attractor.

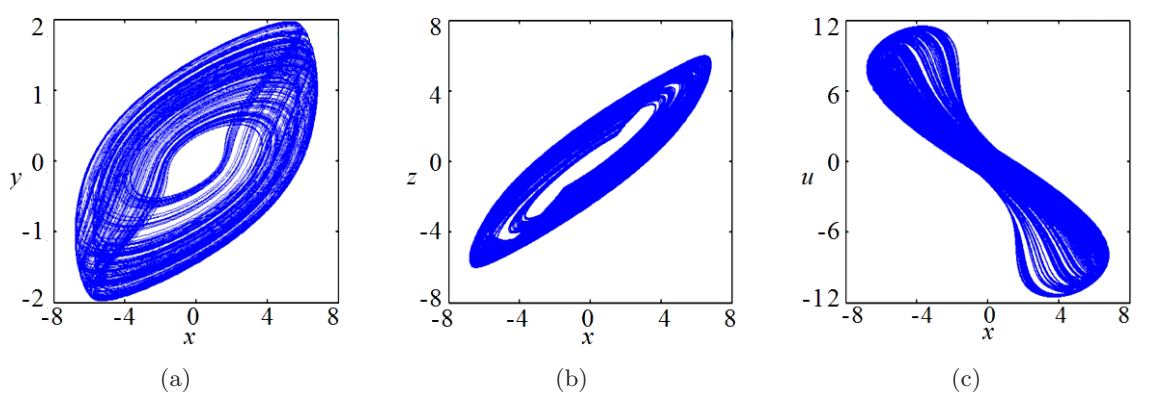

Fig. 8. The phase portraits of typical chaotic attractor when $b = 0.3$: (a) x–y plane, (b) x–z plane and (c) x–u plane.

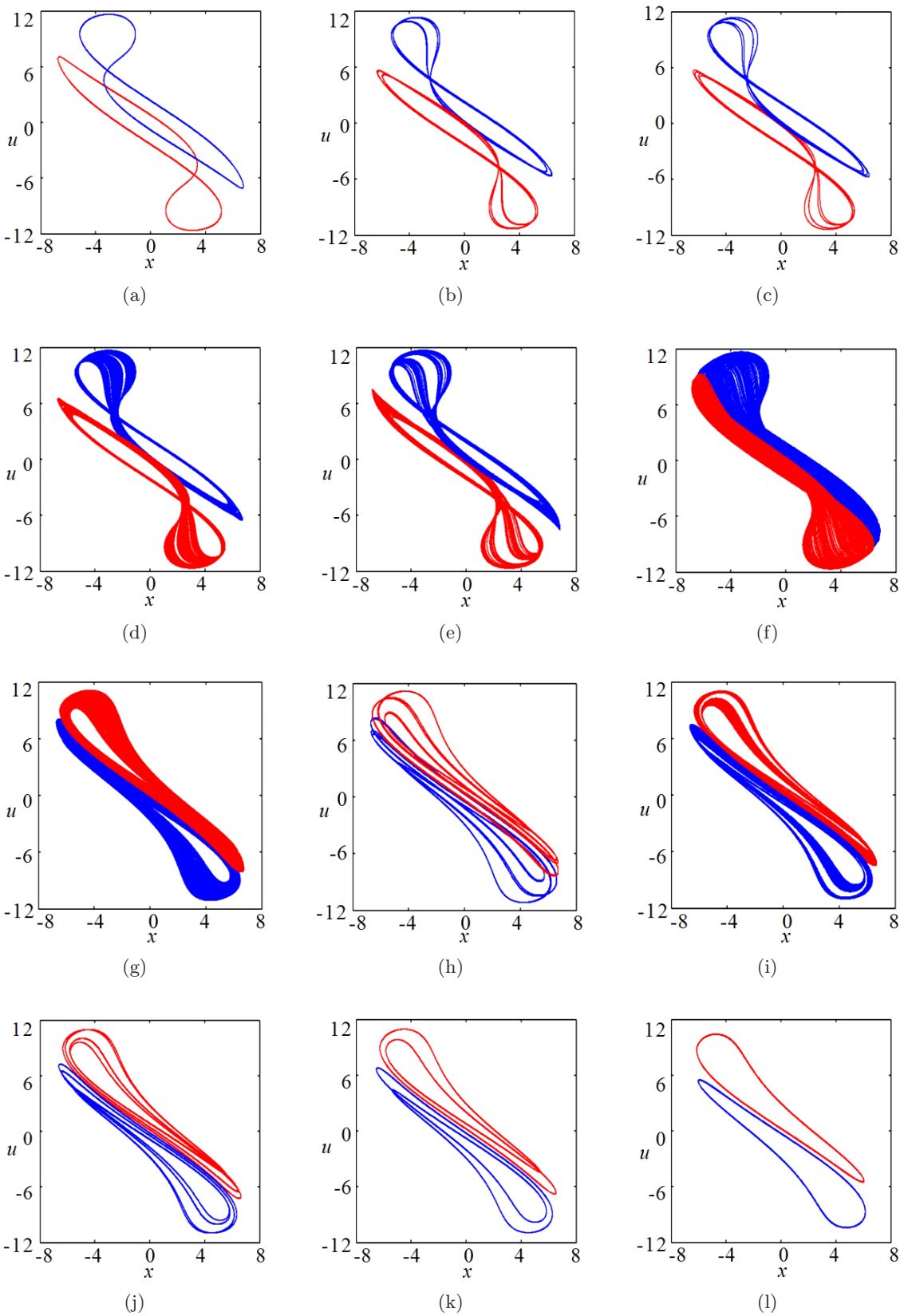

Fig. 9. The coexisting attractors in the x–u plane: (a) period-1 ($b = 0.18$) (b) period-2 ($b = 0.2$), (c) period-4 ($b = 0.201$), (d) chaotic attractor ($b = 0.21$), (e) chaotic attractor ($b = 0.22$), (f) chaotic attractor ($b = 0.24$), (g) chaotic attractor ($b = 0.4$), (h) period-3 ($b = 0.425$), (i) chaotic attractor ($b = 0.43$), (j) period-4 ($b = 0.435$), (k) period-2 ($b = 0.47$) and (l) period-1 ($b = 0.55$).

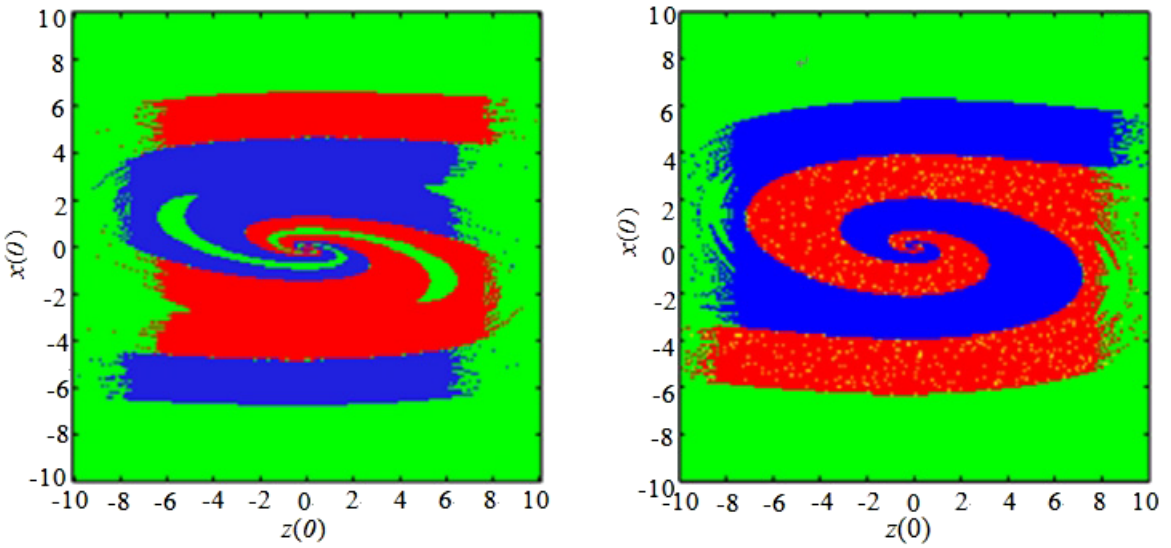

(a) (b)

Fig. 10. Cross-sections of the basin of attraction for $y(0) = u(0) = 0$, corresponding to the asymmetric pair of chaotic attractors (blue and red) and the third coexisting attractor when $b = 0.24$ (yellow): (a) $b = 0.125$ and (b) $b = 0.24$.

4.3. *Antimonotonicity*

It is well known that periodic orbits can be created and then destroyed via reverse period-doubling bifurcation scenarios as a bifurcation control parameter is slowly changing [Dawson *et al.*, 1992]. This type of creation and annihilation of periodic orbits is named as antimonotonicity, and it has been observed in various nonlinear systems such as memristive jerk system [Kengne *et al.*, 2017], the Duffing oscillator [Srinivasan *et al.*, 2009], Chua circuit [Kocarev *et al.*, 1993], laser system [Chlouverakis & Adams, 2006] and series-parallel LC circuit [Manimehan & Philominathan, 2012]. From the bifurcation diagrams in Figs. 3 and 4, the dynamical behaviors can be described as periodic orbits → chaotic orbits → periodic orbits → periodic orbits → chaotic orbits → periodic orbits. As far as we know, antimonotonicity (two full Feigenbaum remerging trees in series) is less observed in the autonomous chaotic systems. Also, in order to demonstrate the phenomenon of antimonotonicity in our system (5) obviously, some bifurcation diagrams as parameter b are varied in the interval [0.1, 0.4] for some discrete values of parameter a are drawn. The simulation results are described in Fig. 12. In light of the graphs in Fig. 12, for $a = 6.6$, two primary bubbles are observed

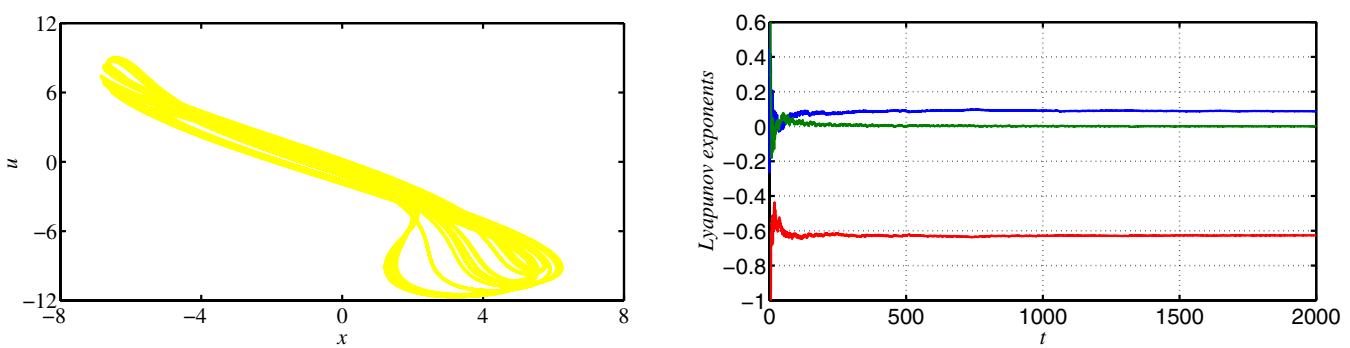

(a) (b)

Fig. 11. The third coexisting attractor when $b = 0.24$ (the initial conditions are $(-0.025125628140704, 0, -4.547738693467337, 0)$): (a) the phase portrait in the x–u plane and (b) the first three Lyapunov exponents.

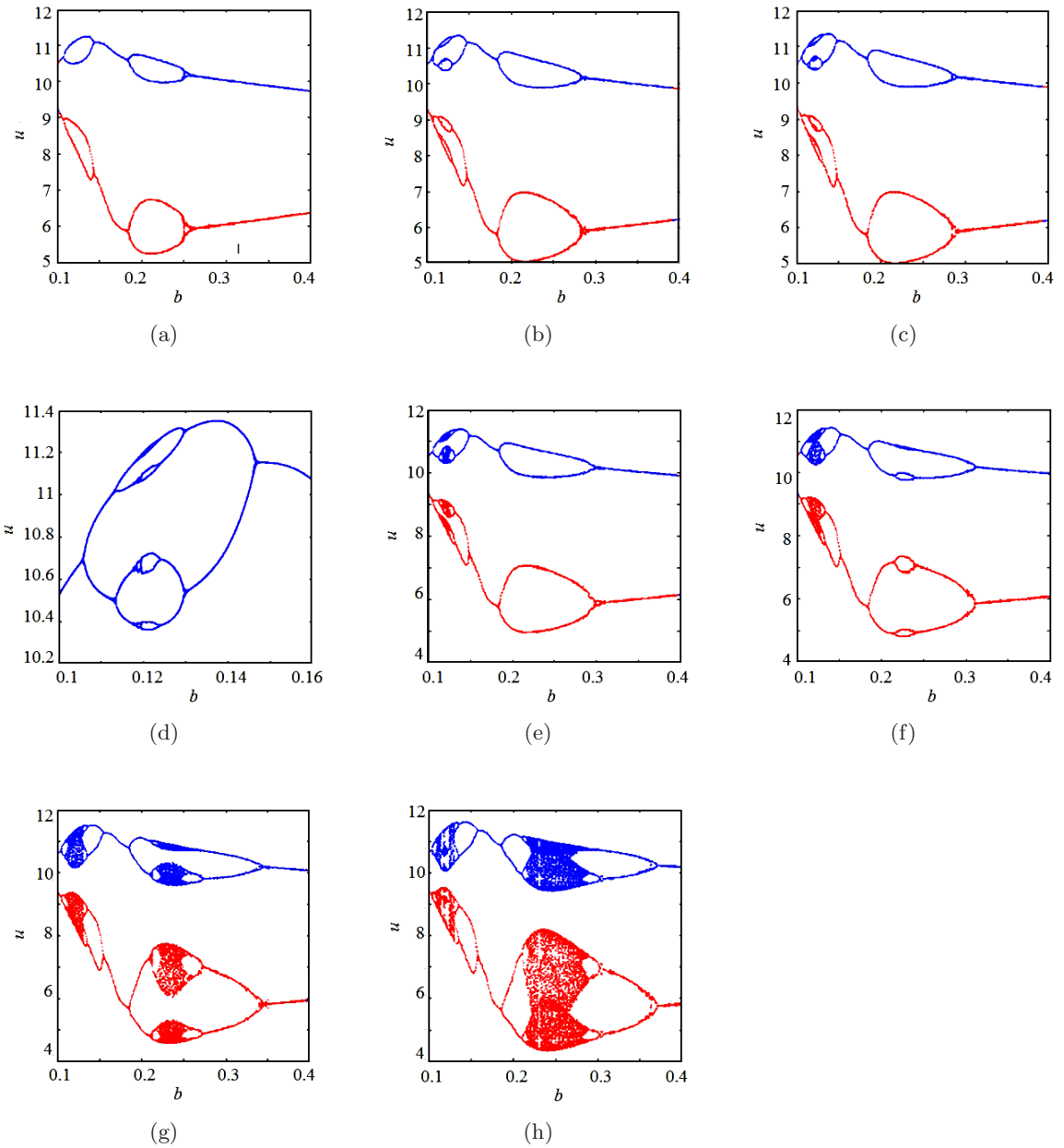

Fig. 12. Bifurcation diagrams showing local maxima of the coordinate u in terms of control parameter b for remerging Feigenbaum tree (bubbling): (a) two primary bubbles for $a = 6.6$, (b) period-4 bubble and period-2 bubble in series at $a = 6.7$, (c) period-8 bubble and period-2 bubble in series at $a = 6.705$, (d) enlargement of (c), (e) a Feigenbaum remerging tree and period-2 bubble in series at $a = 6.75$, (f) a Feigenbaum remerging tree and period-4 bubble in series at $a = 6.8$, (g) and (h) two full Feigenbaum remerging trees at $a = 6.9$ and $a = 7$, respectively.

and the branch develops a stable period-4 bubble and period-2 bubble in series at $a = 6.7$. Similarly, we have a period-8 bubble and period-2 bubble in series at $a = 6.705$, a Feigenbaum remerging tree and period-2 bubble in series at $a = 6.75$, and a Feigenbaum remerging tree and period-4 bubble in series at $a = 6.8$. As a is further increased, two Feigenbaum remerging trees in series (like chaos) finally occur.

5. Hardware Experiments

In order to further research the proposed memristive Twin-T chaotic system shown in Figs. 1 and 2, hardware experiments on a breadboard containing potentiometer, monolithic ceramic capacitor, op-amp TL082 and multiplier AD633JN are made to verify dynamical behaviors of the memristive Twin-T oscillator. The circuit parameters are

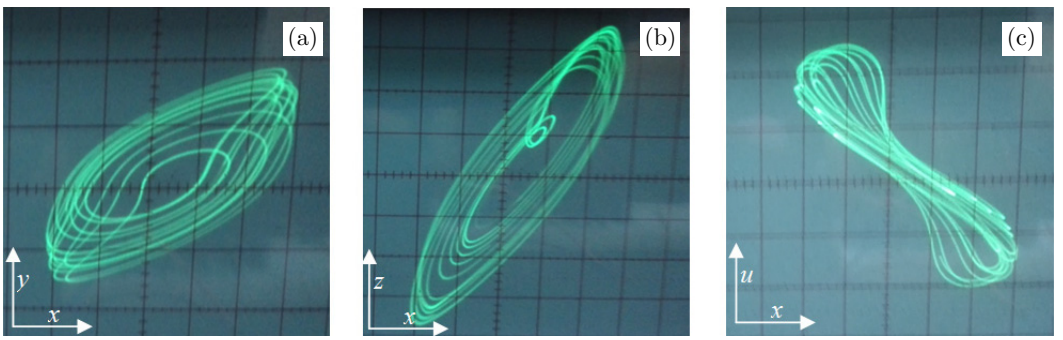

Fig. 13. Experimental measured phase portraits when $R_2 = 333.3\,\mathrm{k\Omega}$, and the scales are $x = 2\,\mathrm{V/div}$, $y = 1\,\mathrm{V/div}$ and $u = 5\,\mathrm{V/div}$.

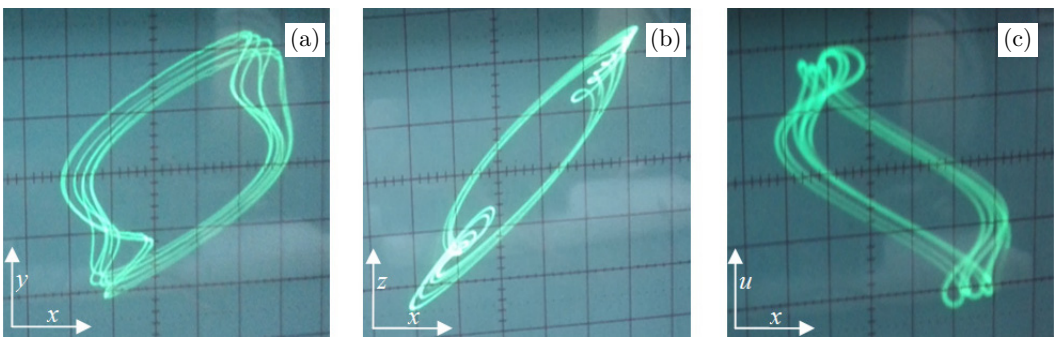

Fig. 14. Experimental measured phase portraits when $R_2 = 909\,\mathrm{k\Omega}$, and the scales are $x = 2\,\mathrm{V/div}$, $y = 1\,\mathrm{V/div}$ and $u = 5\,\mathrm{V/div}$.

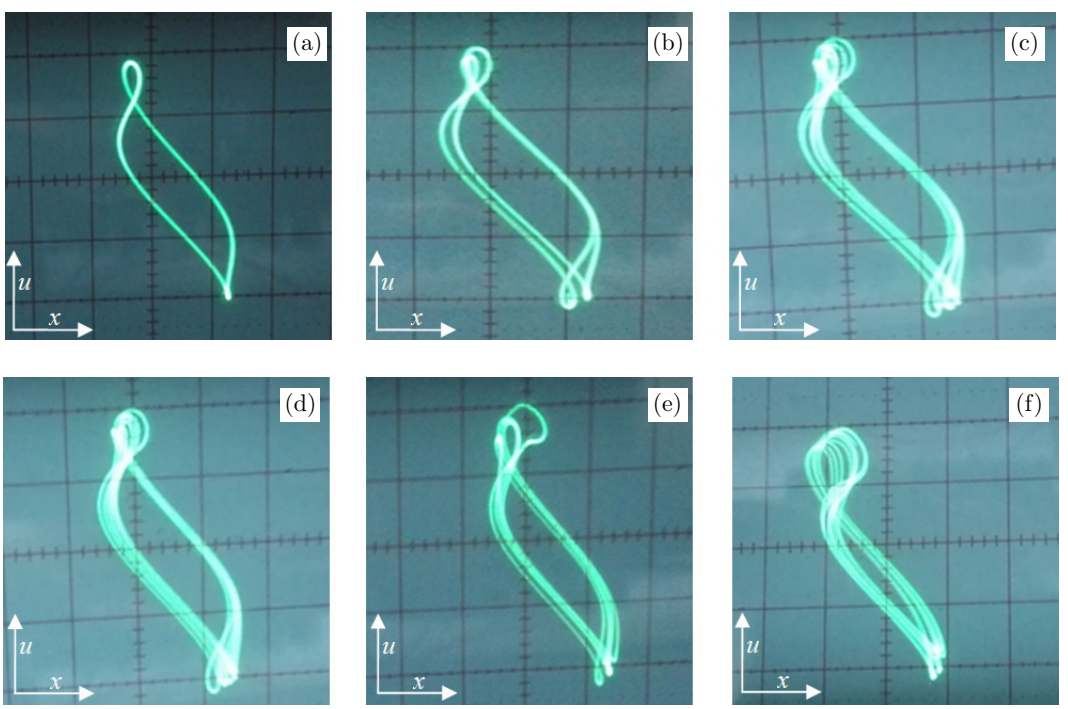

Fig. 15. Experimental measured phase portraits under different R_2. The scales are $x = 2\,\mathrm{V/div}$ and $u = 5\,\mathrm{V/div}$ for all pictures: (a) $R_2 = 1\,\mathrm{M\Omega}$, (b) $R_2 = 990\,\mathrm{k\Omega}$, (c) $R_2 = 964.3\,\mathrm{k\Omega}$, (d) $R_2 = 952\,\mathrm{k\Omega}$, (e) $R_2 = 941.6\,\mathrm{k\Omega}$ and (f) $R_2 = 800\,\mathrm{k\Omega}$.

selected as $C_\varphi = C_1 = C_2 = C_3 = 10\,\text{nF}$, $R_\varphi = 13.3\,\text{k}\Omega$, $R_1 = 28.57\,\text{k}\Omega$, $R_{m1} = 10\,\text{k}\Omega$, $R_{m2} = 100\,\text{k}\Omega$, $R_A = 1\,\text{k}\Omega$, $R_B = 10\,\text{k}\Omega$. And DC power supplies are $\pm 15\,\text{V}$. R_2 is a variable resistance. The experimental results are photographed, as shown in Figs. 13–16. Compared with Figs. 6–9, the experimental results are in accord with simulation results.

By switching on and off the power supply, the coexisting attractors can be obtained. Two coexisting chaotic attractors in the x–u plane when

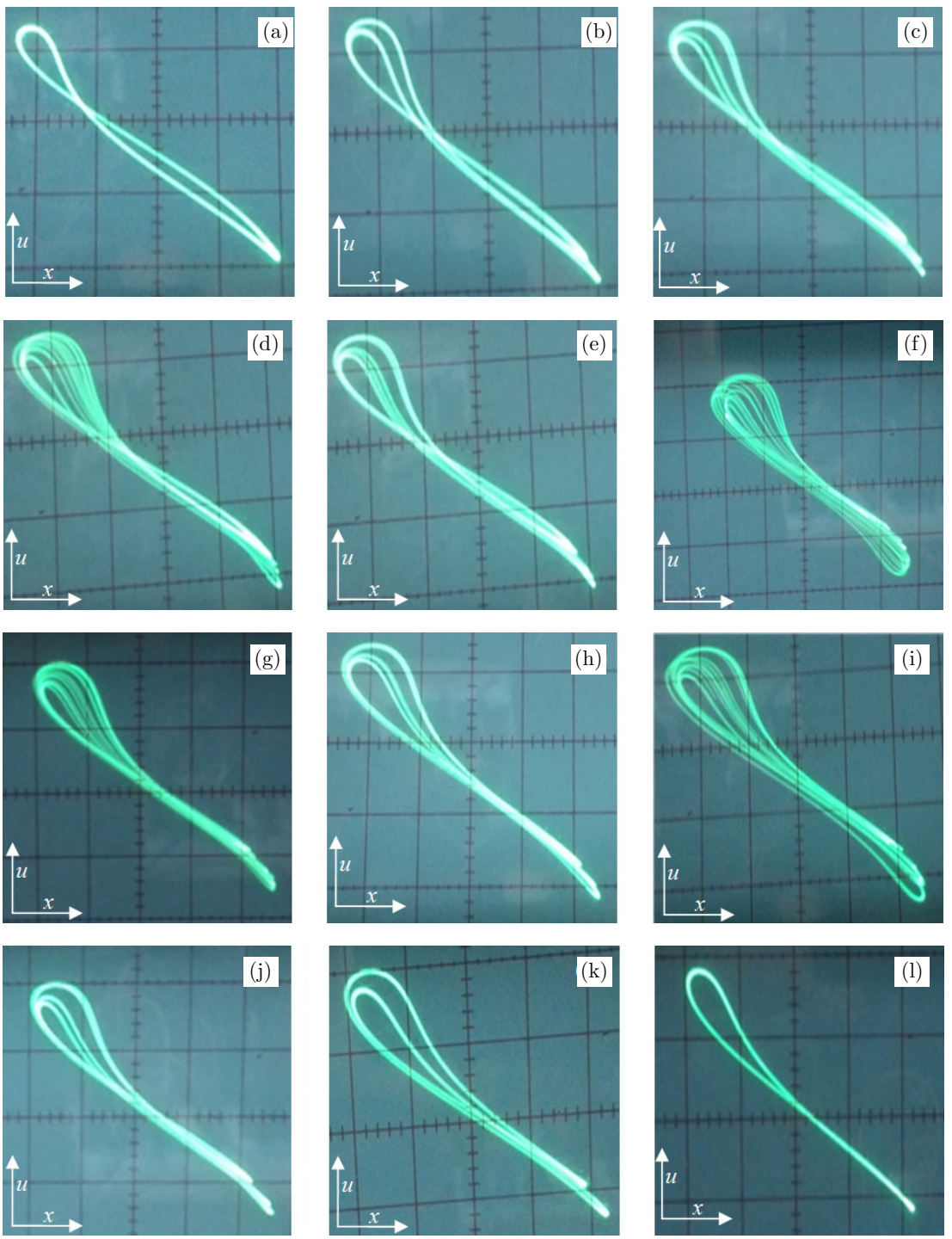

Fig. 16. Experimental measured phase portraits under different R_2. The scales are $x = 2\,\text{V/div}$ and $u = 5\,\text{V/div}$ for all pictures: (a) $R_2 = 555.5\,\text{k}\Omega$, (b) $R_2 = 500\,\text{k}\Omega$, (c) $R_2 = 497.5\,\text{k}\Omega$, (d) $R_2 = 476.1\,\text{k}\Omega$, (e) $R_2 = 454.5\,\text{k}\Omega$, (f) $R_2 = 416.6\,\text{k}\Omega$, (g) $R_2 = 250\,\text{k}\Omega$, (h) $R_2 = 235.29\,\text{k}\Omega$, (i) $R_2 = 232.55\,\text{k}\Omega$, (j) $R_2 = 229.8\,\text{k}\Omega$, (k) $R_2 = 212.7\,\text{k}\Omega$ and (l) $R_2 = 181.8\,\text{k}\Omega$.

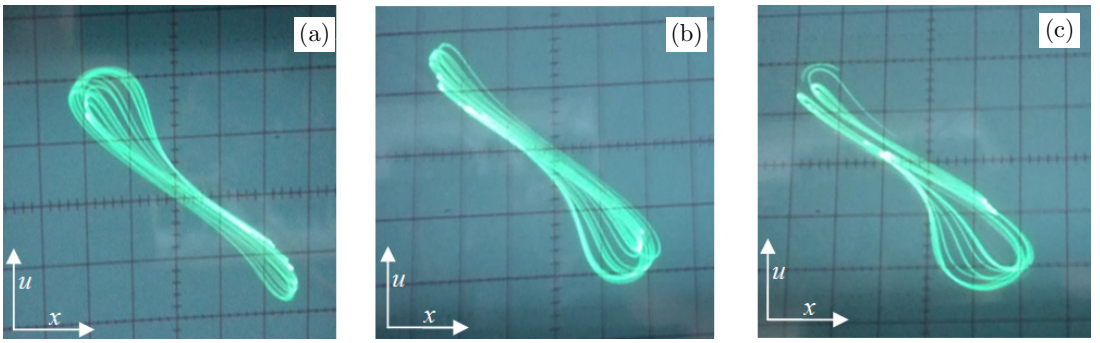

Fig. 17. The coexisting attractors in the x–u plane when $R_2 = 416.6\,\text{k}\Omega$, and the scales are $x = 2\,\text{V/div}$ and $u = 5\,\text{V/div}$ for all pictures.

$R_2 = 416.6\,\text{k}\Omega$ are shown in Fig. 17 (because there are too many figures of coexisting attractors corresponding to Figs. 15 and 16, the case when $b = 0.24$ is selected to verify the existence of coexisting attractors).

6. Random Bit Generator Design and Application

6.1. *Random bit generator design with the memristive Twin-T oscillator*

Chaotic systems are used in random bit generator as entropy source because they are complex and very sensitive. The process of quantized random sequence will directly affect the randomness and complexity of the sequence, and ultimately affect the security of its application system [Yalcin *et al.*, 2004; Akgul *et al.*, 2016]. In this section, the random bit generator design steps are shown in Algorithm 1 as pseudocode.

We set $h = 0.02$, $t_0 = 500$, and the system parameters ($a = 7.5$, $b = 0.35$, $c = 3.5$, $m = 10$, $n = 1$, $k = 0.1$, $g = 0.1$), and the initial conditions are (1 0 0 0). All these processes are based on the above algorithm, the NIST-800-22 statistical tests are used for success of the random bit generator design. The NIST-800-22 tests consist of 16 different tests. The results of the NIST-800-22 tests should be greater than 0.01 for success. Results of NIST-800-22 test for 1 Mbit number series generated with chaotic system are given in Table 2. In Table 2, values are given when x or y or z is -4 for Random Excursions test, and x or y or z is -9 for Random Excursions Variant test. Random Excursions and

Algorithm 1 Random bit generator design algorithm pseudocode

```
Start
Entering parameters and initial condition of memristive Twin-T chaotic system
Determination of the values of h, n and t0 (where n is the length of sequence, t0 is used to bypass the
    transient stage)
Sampling with determination h value
for (i = 1 to length of all data) do
Solving the chaotic system with RK4
Convert float to binary number
Add periodic perturbation
end for
The implementation of NIST tests for bit binary sequency data
if test results == pass then
Successful results
else (test results == false)
Return the previous steps and generate bits again
end if
End
```

Table 2. Random bit generator NIST-800-22 tests for outputs.

Statistical Tests	x P-Value	z P-Value	u P-Value
Frequency (monobit) test	0.646952	0.446060	0.106094
Block frequency test	0.195385	0.759241	0.179463
Runs test	0.145888	0.375304	0.401250
Longest-run test	0.981558	0.558705	0.358571
Binary matrix rank test	0.939268	0.833186	0.444982
Discrete Fourier transform test	0.699927	0.363621	0.378341
Nonoverlapping templates test	0.561791	0.844497	0.317707
Overlapping templates test	0.474914	0.687230	0.454998
Maurers universal statistical test	0.471521	0.131693	0.906409
Linear complexity test	0.625404	0.115927	0.261935
Serial test 1	0.544026	0.665659	0.147126
Serial test 2	0.298254	0.696731	0.340438
Approximate entropy test	0.517227	0.704865	0.063250
Cumulative sums test (left)	0.974737	0.294090	0.098828
Cumulative sums test (right)	0.940276	0.534794	0.190234
Random excursions test ($x = 4$)	0.515355	0.557664	0.078948
Random excursions variant ($x = 9$)	0.332342	0.296133	0.178385

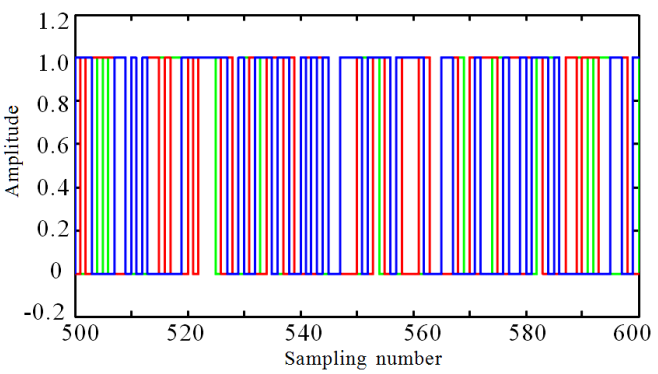

Fig. 18. Three output serials: outputs x(red), outputs z(blue), outputs u(green).

Random Excursions Variant have successful results for the outputs (x, y, z and u), however, y output does not pass all the tests under different pattern-matching of nonoverlapping templates test. From Table 2, it is found that the outputs of x, z and u successfully pass all the tests (all P-values are larger than or equal to 0.01). Figure 18 shows three output serials (we only select partial data to observe clearly). The Twin-T memristive oscillator can be considered as multichannel random bit generator and be used in other engineering and information technology applications that require randomness.

Algorithm 2 Chaos-based image encryption and decryption algorithm pseudocode

1: Start
2: Getting original image P ($M \times N$) to be encrypted
3: Original image data convert to one dimension vector A
4: Getting ready tested random bit sequence B ($8 \times M \times N$) for keys
5: Convert bit sequence B to 8-bit binary sequence C (the length is $M \times N$)
6: **for** $i = 1$ to all original image data **do**
7: 8-bit binary sequence C bit-level xor original image data (one dimension vector A)
8: **end**
9: Encrypted image D
10: Encrypted image data convert to one dimension vector B
11: **for** $i = 1$ to all encrypted image data **do**
12: 8-bit binary sequence C bit-level xor encrypted image data (one dimension vector B)
13: **end**
14: Decrypted image
15: **End**

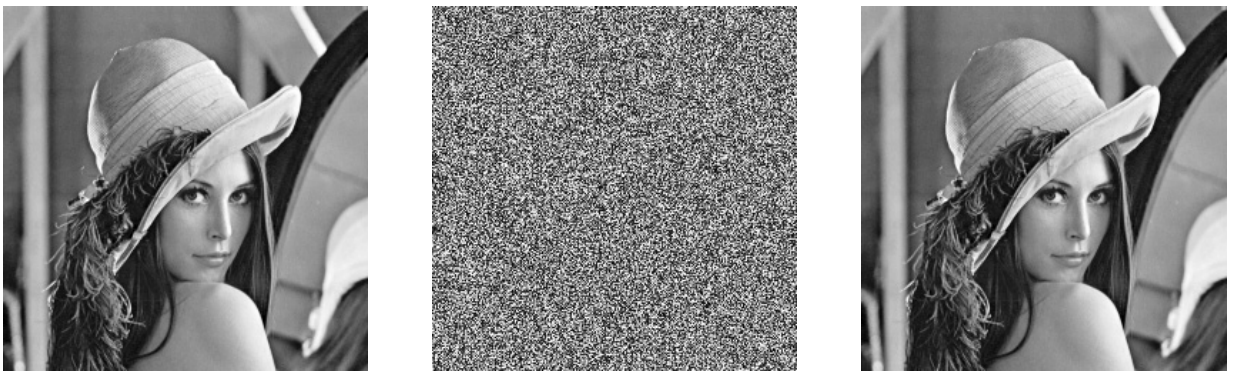

(a) (b) (c)

Fig. 19. Applicability of the encryption and decryption using the proposed random bit generator: (a) original image, (b) encrypted image and (c) decrypted image.

6.2. *Image encryption application*

In this section, an image encryption with random bit generator is realized as an example of chaos-based applications. We select gray scale image Lena (256×256) as an example. The steps of the encryption and decryption process are shown in Algorithm 2.

As shown in Algorithm 2, XOR operator is used for the encryption process. The original image, encrypted image and decrypted image are described in Fig. 18. From Figs. 19(a) and 19(c), there are no distortions between the original and decrypted data. The histogram values are seen in Fig. 20. Obviously, the results in Fig. 20 reveal that the

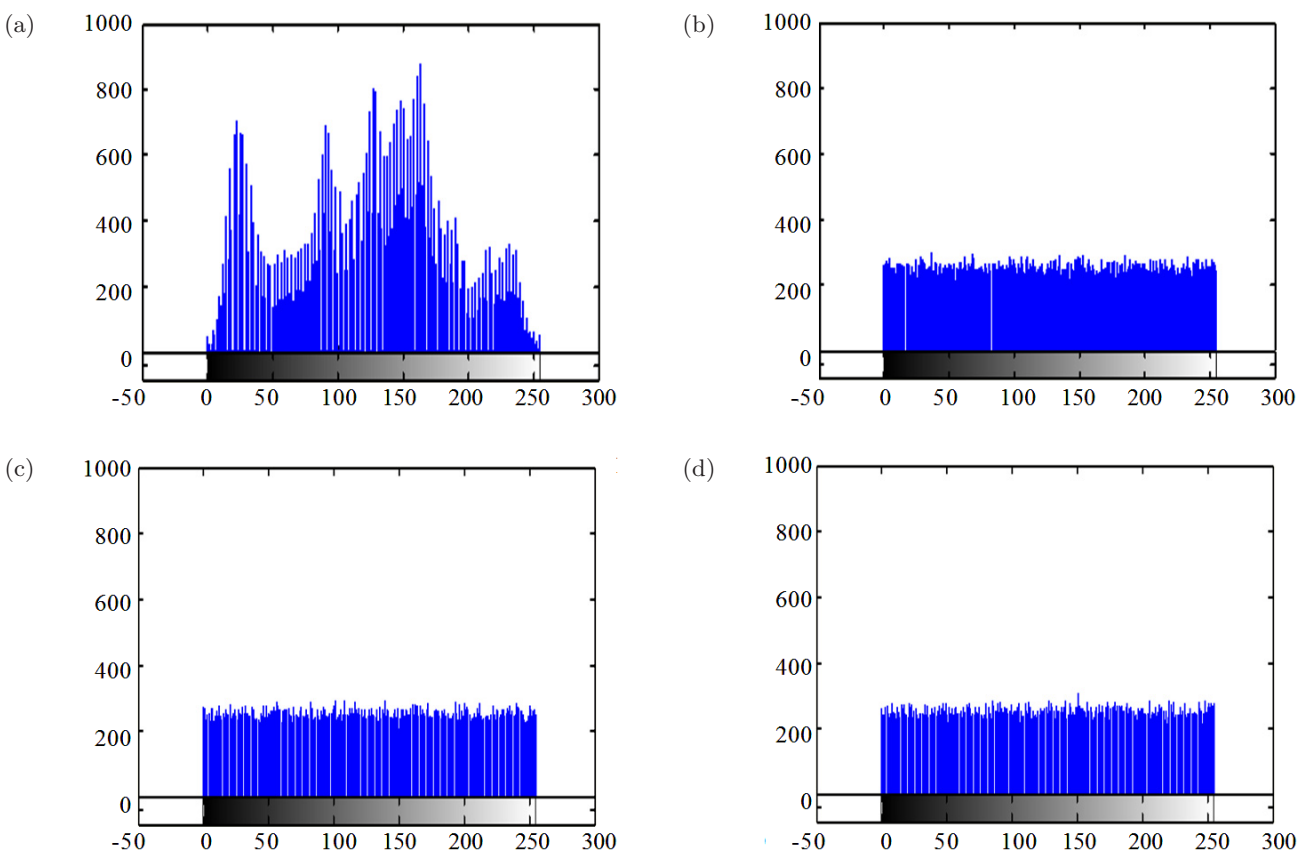

Fig. 20. The histogram of different images: (a) original image, (b) encrypted image with tested random bit sequence x, (c) encrypted image with tested random bit sequence z and (d) encrypted image with tested random bit sequence u.

proposed encrypted images are uniformly distributed as noted in Figs. 20(b)–20(d). This concludes that the proposed encryption algorithm is robust against statistical attacks, and encryptions with different tested random bit sequences were performed successfully.

7. Conclusion

In this paper, we present a simple fourth-order memristive Twin-T oscillator. This circuit was obtained by replacing the resistor in a Twin-T oscillator with generalized flux-controlled memristor. The complex dynamical behaviors are proven via nonlinear dynamics tools, simulations in Matlab, and experiments. Especially, by varying one parameter, various periodic orbits and various chaotic attractors can be obtained by simple fourth-order memristive Twin-T oscillator. At the same time, we observed the phenomena of antimonotonicity and coexisting bifurcation modes. Random bit generator for signal application is proposed, and numerical results illustrate the usefulness of the random bit generator. Furthermore, image encryptions are carried out with the random bit sequence designed here. The proposed circuit with inductor-free is suitable for IC design and may be helpful for chaos-based communication and electronic measurement systems.

Acknowledgments

This work is supported by the National Natural Science Foundation of China (No. 61571185), the Natural Science Foundation of Hunan Province, China (No. 2016JJ2030), the Open Fund Project of Key Laboratory in Hunan Universities (No. 15K027), Scientific Research Fund of Hunan University of Science and Engineering (No. 17XKY070), and Scientific Research Fund of Hunan Provincial Education Department (Nos. 12A054 and 16C0683).

References

Akgul, A., Calgan, H., Koyuncu, I., Pehlivan, I. & Istanbullu, A. [2016] "Chaos-based engineering applications with a 3D chaotic system without equilibrium points," *Nonlin. Dyn.* **84**, 481–495.

Bao, B. C., Jiang, P., Wu, H. G. & Hu, F. W. [2015] "Complex transient dynamics in periodically forced memristive Chua's circuit," *Nonlin. Dyn.* **79**, 2333–2343.

Bao, B. C., Jiang, T., Xu, Q., Chen, M., Wu, H. G. & Hu, Y. [2016] "Coexisting infinitely many attractors in active band-pass filter-based memristive circuit," *Nonlin. Dyn.* **86**, 1711–1723.

Bao, B. C., Jiang, T., Xu, Q., Chen, M., Wu, H. G. & Hu, Y. [2017a] "Two-memristor-based Chua's hyperchaotic circuit with plane equilibrium and its extreme multistability," *Nonlin. Dyn.* **60**, 1–15.

Bao, B. C., Wang, N., Xu, Q., Wu, H. G. & Hu, Y. H. [2017b] "A simple third-order memristive band pass filter chaotic circuit," *IEEE Trans. Circuits Syst.-II*: *Express Briefs* **64**, 977–981.

Chen, M., Li, M. Y., Yu, Q., Bao, B. C., Xu, Q. & Wang, J. [2015] "Dynamics of self-excited attractors and hidden attractors in generalized memristor-based Chua's circuit," *Nonlin. Dyn.* **81**, 215–226.

Chlouverakis, K. E. & Adams, M. J. [2006] "Antimonotonicity and maximal complexity in optically injected two-section lasers: Numerical analysis of a Toda oscillator system," *IEEE J. Selected Top. Quant. Electron.* **12**, 398–404.

Chua, L. O. [1971] "Memristor — The missing circuit element," *IEEE Trans. Circuit Th.* **18**, 507–519.

Chua, L. O. & Kang, S. M. [1976] "Memristive devices and systems," *Proc. IEEE* **2**, 209–223.

Corinto, F. & Forti, M. [2017] "Memristor circuits: Flux charge analysis method," *IEEE Trans. Circuits Syst.-I*: *Reg. Papers* **63**, 1997–2009.

Dawson, S. P., Grebogi, C., Yorke, J. A., Kan, I. & Kocak, H. [1992] "Antimonotonicity: Inevitable reversals of period-doubling cascades," *Phys. Lett. A* **162**, 249–254.

Duan, S., Hu, X., Dong, Z., Wang, L. & Mazumder, P. [2015] "Memristor-based cellular nonlinear/neural network: Design, analysis, and applications, neural networks and learning systems," *IEEE Trans. Neural Netw. Learn. Syst.* **26**, 1202–1213.

Elwakil, A. S. & Kennedy, M. P. [2000] "Chua's circuit decomposition: A systematic design approach for chaotic oscillators," *J. Franklin Inst.* **337**, 251–256.

Iu, H. H. C., Fitch, A. L. & Yu, D. S. [2010] "Chaos in a Twin-T circuit," *Int. J. Bifurcation and Chaos* **20**, 3283–3293.

Iu, H. H. C., Yu, D. S., Fitch, A. L., Sreeram, V. & Chen, H. [2011] "Controlling chaos in a memristor based circuit using a Twin-T notch filter," *IEEE Trans. Circuits Syst.-I*: *Reg. Papers* **58**, 1337–1343.

Kengne, J., Negou, A. N. & Tchiotsop, D. [2017] "Antimonotonicity, chaos and multiple attractors in a novel autonomous memristor-based jerk circuit," *Nonlin. Dyn.* **88**, 2589–2608.

Keuninckx, L., Sande, G. V. D. & Danckaert, J. [2015] "Simple two-transistor single-supply resistor-capacitor chaotic oscillator," *IEEE Trans. Circuits Syst.-II*: *Express Briefs* **62**, 891–895.

Kocarev, L., Halle, K., Eckert, K. & Chua, L. [1993] "Experimental observation of antimonotonicity in Chua's circuit," *Int. J. Bifurcation and Chaos* **3**, 1051–1055.

Li, C. B. & Sprott, J. C. [2013] "Multistability in a butterfly flow," *Int. J. Bifurcation and Chaos* **23**, 1350199-1–10.

Li, Z. J. & Zeng, Y. C. [2013] "A memristor oscillator based on a Twin-T network," *Chin. Phys. B* **22**, 4040502-1–6.

Li, C., Song, Y., Wang, F. Y., Liang, Z. Y. & Zhu, B. Y. [2015] "Chaotic path planner of autonomous mobile robots based on the standard map for surveillance missions," *Math. Probl. Eng.* **2015**, 1–11.

Li, Y. P., Wang, C. H. & Chen, H. [2017] "A hyper-chaos-based image encryption algorithm using pixel-level permutation and bit-level permutation," *Opt. Lasers Engin.* **90**, 238–246.

Lin, Z., Yu, S. M., Li, C. B., Lü, J. & Wang, Q. [2016] "Design and smartphone-based implementation of a chaotic video communication scheme via WAN remote transmission," *Int. J. Bifurcation and Chaos* **26**, 1650158-1–8.

Ma, J., Wu, F., Ren, G. & Tang, J. [2017] "A class of initials-dependent dynamical systems," *Appl. Math. Comput.* **298**, 65–76.

Manimehan, I. & Philominathan, P. [2012] "Composite dynamical behaviors in a simple series-parallel LC circuit," *Chaos Solit. Fract.* **45**, 1501–1509.

Morgul, O. [1995] "Wien bridge based RC chaos generator," *Electron. Lett.* **31**, 2058–2059.

Namajunas, A. & Tamasevicius, A. [1996] "Simple RC chaotic oscillator," *Electron. Lett.* **32**, 945–846.

Ren, H. P., Bai, C., Huang, Z. Z. & Grebogi, C. [2017] "Secure communication based on hyperchaotic Chen system with time-delay," *Int. J. Bifurcation and Chaos* **27**, 1750076-1–15.

Soudry, D., Di, C. D., Gal, A., Kolodny, A. & Kvatinsky, S. [2015] "Memristor-based multilayer neural networks with online gradient descent training," *IEEE Trans. Neural Netw. Learn. Syst.* **26**, 2408–2421.

Srinivasan, K., Thamilmaran, K. & Venkatesan, A. [2009] "Effect of nonsinusoidal periodic forces in Duffing oscillator: Numerical and analog simulation studies," *Chaos Solit. Fract.* **40**, 319–330.

Strukov, D. B., Snider, G. S., Stewart, D. R. & Williams, R. S. [2008] "The missing memristor found," *Nature* **453**, 80–83.

Strukov, D. B. [2016] "Endurance-write-speed tradeoffs in nonvolatile memories," *Appl. Phys. A* **122**, 302.

Wang, C. H., Liu, X. M. & Xia, H. [2017] "Multi-piecewise quadratic nonlinearity memristor and its $2N$-scroll and $2N + 1$-scroll chaotic attractors system," *Chaos* **27**, 033114.

Wu, H. G., Bao, B. C., Liu, Z., Xu, Q. & Jiang, P. [2016] "Chaotic and periodic bursting phenomena in a memristive Wien-bridge oscillator," *Nonlin. Dyn.* **83**, 893–903.

Wu, R. P. & Wang, C. H. [2016] "A new simple chaotic circuit based on memristor," *Int. J. Bifurcation and Chaos* **26**, 1650145-1–11.

Xu, Q., Lin, Y., Bao, B. C. & Chen, M. [2016] "Multiple attractors in a non-ideal active voltage-controlled memristor based Chua's circuit," *Chaos Solit. Fract.* **83**, 186–200.

Yalcin, M. E., Suykens, J. A. K. & Vandewalle, J. [2004] "True random bit generation from a double-scroll attractor," *IEEE Trans. Circuits Syst.-I*: *Reg. Papers* **51**, 1395–1404.

Yu, D. S., Iu, H. H. C., Fitch, A. L. & Liang, Y. [2014a] "A floating memristor emulator based relaxation oscillator," *IEEE Trans. Circuits Syst.-I*: *Reg. Papers* **61**, 2888–2896.

Yu, Q., Bao, B. C., Hu, F. W., Xu, Q., Chen, M. & Wang, J. [2014b] "Wien-bridge chaotic oscillator based on fisrt-order generalized memristor," *Acta Phys. Sin.* **63**, 240505-1–11.

Yuan, F., Wang, G. Y. & Wang, X. W. [2016] "Extreme multistability in a memristor-based multi-scroll hyper-chaotic system," *Chaos* **26**, 073107.

Zhou, L., Wang, C. H. & Zhou, L. L. [2016] "Generating hyperchaotic multi-wing attractor in a 4D memristive circuit," *Nonlin. Dyn.* **85**, 2653–2663.